

Article

Okra Micro-Cellulose Crystal (MCC) and Micro-Clay Composites for the Remediation of Copper, Nickel, and Dye (Basic Yellow II) from Wastewater

Anika Amir Mohana ¹, Md. Aminur Rahman ^{2,3,*} , Md. Hafezur Rahaman ¹ , Mohd. Maniruzzaman ¹, S. M. Farhad ¹, Md Meftaul Islam ⁴ , Md. Sirajul Islam Khan ⁴  and Md. Zahid Parvez ⁵

¹ Department of Applied Chemistry and Chemical Engineering, Islamic University, Kushtia 7003, Bangladesh

² Zonal Laboratory, Department of Public Health Engineering (DPHE), Jashore 7400, Bangladesh

³ Global Center for Environmental Remediation (GCER), College of Engineering, Science and Environment, The University of Newcastle, Callaghan, NSW 2308, Australia

⁴ Department of Agricultural Chemistry, Sher-e-Bangla Agricultural University, Dhaka 1207, Bangladesh

⁵ Department of Public Health Engineering (DPHE), Jashore Division, Jashore 7400, Bangladesh

* Correspondence: md.aminur.rahman@uon.edu.au

Abstract: Water pollution by contaminants such as toxic metals and dyes is now a major concern due to their high toxicity and persistence in the environment. Advances in nanotechnology have enabled the use of micro/nanomaterials to treat and purify water in various industries. In this study, Bijoypur clay was modified with ethyldiamine and incorporated into an okra fiber (*Abelmoschus esculentus*) micro-cellulose crystal (MCC) to produce a composite that could absorb copper (Cu), nickel (Ni), and dyes like basic yellow (II) from industrial wastewater. Composites were prepared using different percentages of MCC and clay. Atomic absorption spectroscopy (AAS) was used to determine the concentrations of Cu and Ni whereas a UV-Visible spectrophotometer measured the absorbance of basic yellow (II). The synthesized composites were extensively characterized using a range of techniques including thermogravimetry (TG) and differential thermogravimetry (DTG), Fourier transform infrared spectroscopy (FTIR), scanning electron microscopy (SEM), and X-ray diffraction (XRD). Results show that both the MCC and clay could absorb Cu, Ni, and basic yellow (II) from the contaminated wastewater. The MCC and clay composite showed the maximum efficiency of metals removal, which was up to 95% (24 mg/g) for Cu at pH 6, 20 min contact time, 2 g/L adsorbent dose, and 100% (31 mg/g) for Ni at pH 8, 60 min contact time, and 2 g/L adsorbent dose, respectively, at the initial concentration of 50 mg/L. The maximum dye uptake capacity of 85% (19 mg/g) was observed by the MCC and clay composite under optimized conditions at the initial concentration of 50 mg/L, pH 8, 30 min contact time, and 1 g/L adsorbent dose compared to the pure clay, which had an efficiency up to 26% for Cu and 24% for dye removal. All of the results indicate that incorporating clay into MCC increases the absorption capacity of contaminants from wastewater, which could be more effective for environmental applications compared to untreated cellulose.

Keywords: micro-cellulose; pollutants; dye; clay; micro-composite; remediation; wastewater



Citation: Mohana, A.A.; Rahman, M.A.; Rahaman, M.H.; Maniruzzaman, M.; Farhad, S.M.; Islam, M.M.; Khan, M.S.I.; Parvez, M.Z. Okra Micro-Cellulose Crystal (MCC) and Micro-Clay Composites for the Remediation of Copper, Nickel, and Dye (Basic Yellow II) from Wastewater. *Reactions* **2023**, *4*, 342–358. <https://doi.org/10.3390/reactions4030021>

Academic Editor: Diogo M.F. Santos

Received: 11 January 2023

Revised: 19 June 2023

Accepted: 27 June 2023

Published: 4 July 2023



Copyright: © 2023 by the authors. Licensee MDPI, Basel, Switzerland. This article is an open access article distributed under the terms and conditions of the Creative Commons Attribution (CC BY) license (<https://creativecommons.org/licenses/by/4.0/>).

1. Introduction

Water is one of the world's most precious natural resources. Only 1% of the planet's water is easily accessible drinking water [1]. The deficiency in water quality is of growing global concern in the twenty-first century [2,3]. The environment, aquatic life, animals, and humans are in serious trouble due to water being contaminated by heavy metals [4,5]. Unregulated industrialization and urbanization have created a severe threat to water bodies worldwide [6], and hence it is very important to remove heavy metal ions from polluted water [7–9]. However, Bangladesh is a developing country where its safe drinking water resources are diminishing day by day. The surface water of Dhaka, the capital city

of Bangladesh, and those of other metro cities has become highly polluted due to the unsystematic discharge of raw waste containing potentially toxic metals and dyes from textiles, tanneries [10], pesticides, fertilizers, municipalities, and other industries [11]. A large population, poor drainage system, and urban encroachment are all making the water pollution worse [12].

The current WHO tolerance levels of copper (Cu) and nickel (Ni) in groundwater are 2.0 mg/L and 0.07 mg/L, whereas in Bangladesh, the drinking water guidelines are 1.0 mg/L and 0.1 mg/L, respectively [13,14]. Thus, there is a high demand to clean up Cu, Ni and dye-enriched water sources to below the recommended values.

Some techniques such as adsorption, chemical precipitation, ion exchange, conventional coagulation, reverse osmosis, electro dialysis, and electrolysis can remove water containing dissolved materials such as hydrogen sulfide, parasites, bacteria, lead nitrate, non-dissolved particulate matter, and other micropollutants from water and industrial wastewater [15,16]. Due to its simplicity and cost efficiency, adsorption holds considerable promise among the many technologies available for the removal of heavy metal ions from aqueous solutions [17–21]. However, most adsorbents such as activated carbons, biochars [22,23], clays [24], and zeolites [25] show weak binding affinities toward metal ions. High efficiency can be achieved by introducing complex functional groups that improve the metal uptake capacity into these porous materials [26–29]. Although there are some restrictions because of its agglomeration nature, micro-cellulose has a high surface area and a great capacity to purify water. By converting micro-materials to micro-composites, this agglomeration of micro-cellulose can be reduced.

Both from a scientific point of view and from the perspective of developing novel structural and functional macroscopic materials, renewable resource-based micro-materials are currently garnering a lot of interest [30,31]. Cellulose is the most abundant natural macromolecule, and can be derived from plants, animals, and even marine organisms on Earth [32]. Roughly 15–30% of the dry mass in the primary cell wall and more than 40% in the secondary cell wall of plants is cellulose [33]. Thus, many investigations have concentrated on the top-down isolation of nanocellulose from abundant green resources including various species of wood [34], pea hull [35], bamboo [36], sisal [37], soy hulls [38], branch-barks of mulberry [39], cotton [40], pineapple leaf [35], hemp [41], coconut husk [42], banana rachis [43], okra [44], sugar beet [45], rice straw [46], oat straw, wheat straw [38], corn straw [47], needles grass [48], and so on. MCC are rod-like nanoparticles, and depending on the preparation route and origin of the cellulose, they vary in length between 100 and 2000 μm , having diameters ranging between 1 and 10 μm [49]. Strong acid hydrolysis is well-known for isolating micro-cellulose from cellulose, which removes the amorphous regions of cellulose fiber and produces micro-size fibrils [50]. Sulfuric acid reacts with the cellulose surface hydroxyl groups to form sulfate half-esters, which leads to negatively charged, and thus electrostatically stabilized, MCC particles [49]. For the selective removal of contaminants from industrial and drinking water, micro-cellulose is a very promising material for high-performance membranes and filters because of its chemical inertness, high strength, hydrophilic surface chemistry, and excessive surface area.

A considerable amount of information is available in the literature [51,52] on organo-clays, natural sediments and aquifer materials, soils, montmorillonite, and kaolinite as adsorbents of various organic substances. There are three basic types of clays: kaolinite, smectites (e.g., montmorillonite), and micas (e.g., illite) [53]. A huge reserve of white clay exists in Bijoypur, in the Netrokona District in Bangladesh, which is kaolinite in nature [54]. Chemically, kaolinite is a 1:1 layer sheet structured hydrated aluminum silicate with a very fine particle size with single a silicon–oxygen (Si–O) tetrahedral layer and a single alumina [Al_2O_3] octahedral layer (or expressed in another way, [Si_2O_5] $^{2-}$ sheet and [$\text{Al}_2(\text{OH})_4$] $^{2+}$ sheet) with pseudo-hexagonal symmetry, bonded together through sharing of apical oxygen that exists alternately. Its theoretical formula is $\text{Si}_2\text{Al}_2\text{O}_5(\text{OH})_4$ (other formulas are $\text{Al}_2\text{O}_3 \cdot 2\text{SiO}_2 \cdot 2\text{H}_2\text{O}$ and $\text{Al}_2\text{O}_7\text{Si}_2 \cdot 2\text{H}_2\text{O}$), which has a molecular weight of 258.16 g/mol [55,56]. Clay minerals are universal in nature and they have been used

extensively as sorbents, catalysts, and catalyst supports [57,58]. They have been tested for the selective removal of organic and inorganic pollutants from aqueous media [59] because they have a high sorption capacity, localized acidity, shape specificity, restricted movement of water molecules, etc. [60]. To attain magnetic nanoparticles, clay minerals can be used as a matrix because of its unique physicochemical properties and high cation exchange capability including large chemically active surface area, mechanical and thermal stability, and unusual interlamellar surfaces [61–63].

Preference has been given to polymer–clay micro-composites for water purification purposes. The objective of this study was to evaluate the effectiveness of a MCC and clay composite to enhance the quality of contaminated water by removing Cu, Ni, and dye. The specific aims of this work were to find a solution to the water pollution problem by using agricultural waste to make this cost effective. For this end, a range of techniques including thermogravimetry (TG) and differential thermogravimetry (DTG), Fourier transform infrared spectroscopy (FTIR), scanning electron microscopy (SEM), and X-ray diffraction (XRD) were applied to characterize the synthesized composites, specifically to determine the potential of the composite materials. This cost-effective treatment process can be deployed instead of conventional or costly methods as it is environmentally friendly and economically feasible.

2. Experimental

2.1. Reagents

All stock solutions were prepared from the analytical grade reagent (AR). Freshly prepared deionized distilled water was used in all of the experiments. Acetic acid (CH_3COOH) and sulfuric acid (H_2SO_4) were obtained from BDH England, while sodium acetate (CH_3COONa), basic yellow (II), ethyldiamine [$\text{C}_2\text{H}_4(\text{NH}_2)_2$], sodium hydroxide (NaOH), and sodium chlorite (NaClO_2) were also sourced from BDH England.

2.2. Preparation of MCC

A total of 20 gm okra fiber was scoured for 2 h in a solution containing 5 gm L^{-1} detergent in a 2 L beaker. The ratio of the fiber to solution was 1:50 during scouring. Finally, the fiber was thoroughly washed with distilled water several times and dried at 80–90 °C in an electric oven [64]. The fibers were treated in a 17.5% NaOH solution (fiber:NaOH solution = 1:15) at room temperature for 2 h [37], followed by washing continuously with deionized water and kept dry at 105 °C in an electric oven [64]. The alkali-treated fiber was dipped into the 0.7% NaClO_2 in 250 mL deionized water at 90 °C for 2 h at pH 4, which was neutralized with a 5% acetic acid solution. This was followed by washing with deionized water and drying at 100 °C for 6 h [65]. The acid hydrolysis was carried out using a (60 wt.%) H_2SO_4 solution (fiber:liquor = 1:10 to obtain the maximum amount yield) at 45 °C under continuous stirring conditions [66]. After 50 min, it was centrifuged at 4000 rpm [67] for 40 min. The solid fraction was washed by distilled water until a constant pH 7.0 was obtained [37,68]. Figure 1 represents the preparation of MCC from okra cellulose.

2.2.1. Collection and Modification of Clay

The clay sample collected from Bijoypur mainly belongs to the kaolinite type of clay with small amounts of quartz and trace amounts of illite and chlorite. Bijoypur clay was treated with 5% ethyldiamine (to make the clay rough enough to adsorb metal ions) for 24 h to remove the organic materials and increase the hydrophobicity of the clay [69]. Afterward, the solution clay was oven dried at 105 °C and preserved in a desiccator.

2.2.2. Preparation of Composite

The clay and MCC were dispersed or diluted with alcohol and mixed as different ratios at 100, 90, 80, 70, and 60 wt. % (clay/micro-cellulose). The mixture was homogenized using a process homogenizer for 1 h and then stirred for 1 day using a magnetic stirrer at room

temperature and filtered. The filtered MCC–clay sheet was put into a column resemble mold for 2 days at room temperature [70]. The dried sheet was pressed by hand for 10 min. Then, the prepared MCC–clay composite was transferred into a filtration column, as shown in Figure 2.

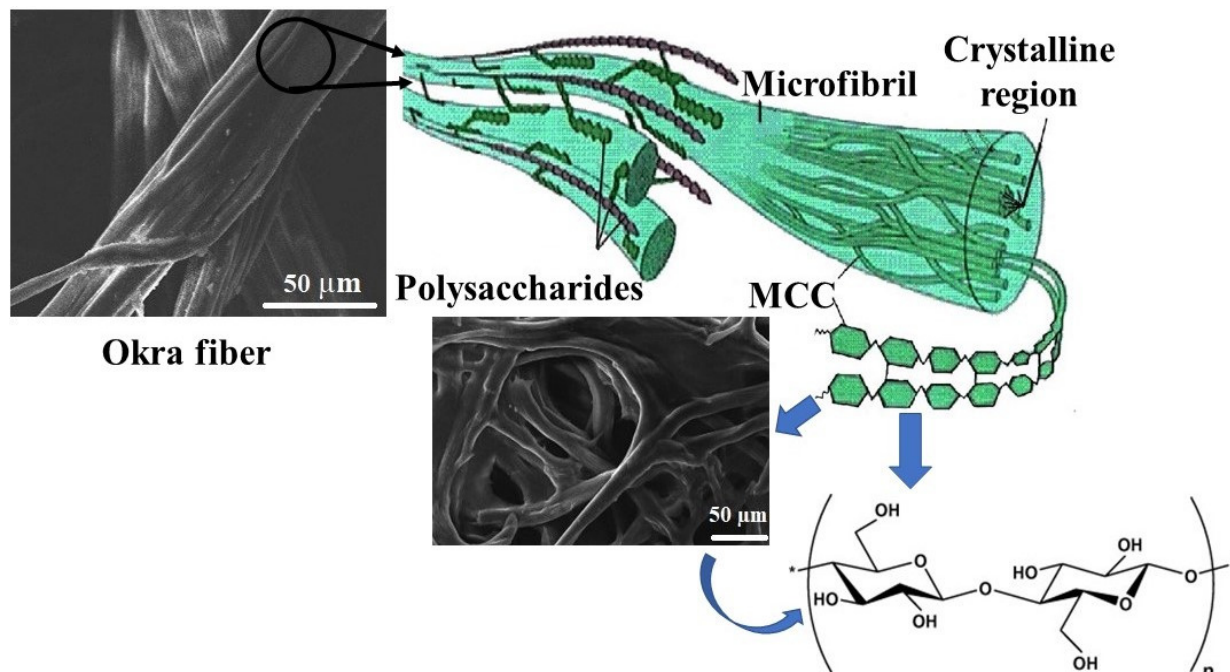


Figure 1. Preparation of the micro-cellulose crystal (MCC) from the cellulose of okra fiber.

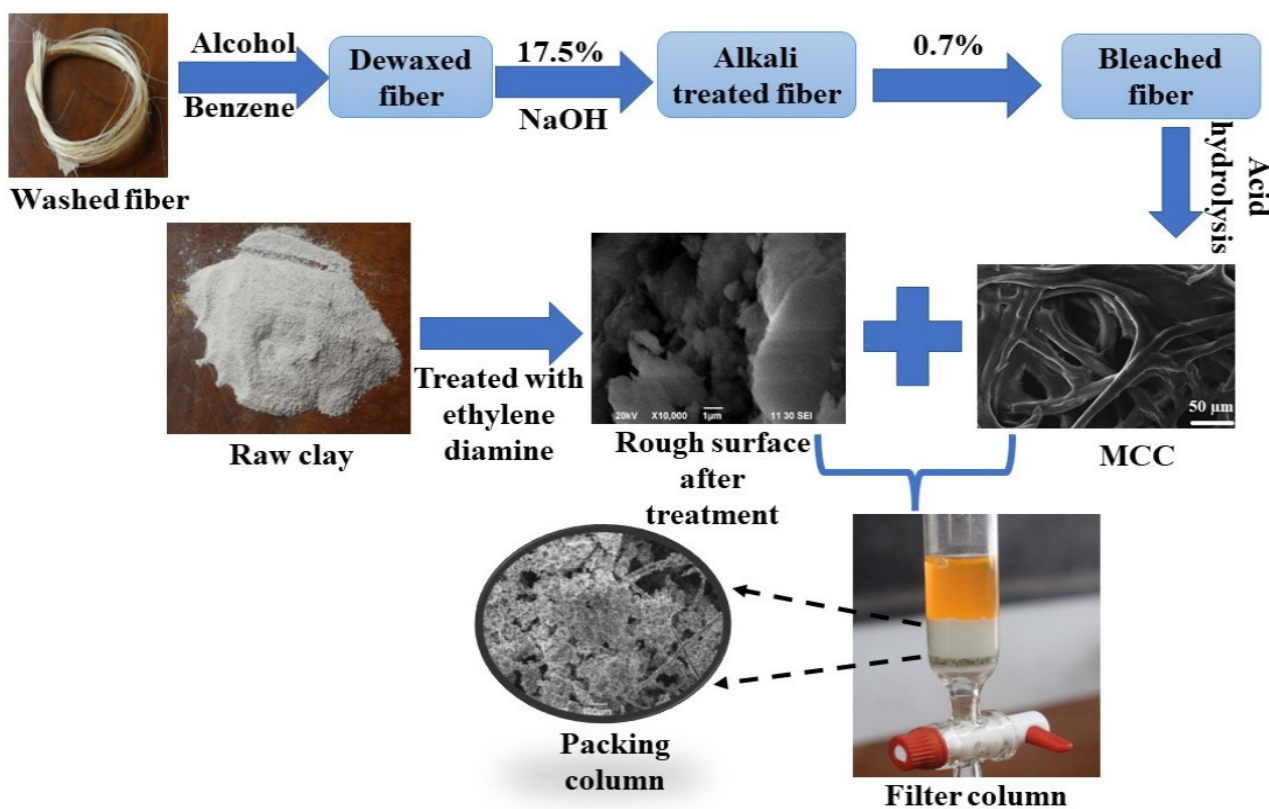


Figure 2. Schematic diagram of the column preparation by the micro-cellulose crystal (MCC) and clay.

2.2.3. Sample Preparation

Five types of columns (Table 1) were prepared by mixing different ratios to clay and micro-cellulose in order to test the metal and dye removal efficacy from the wastewater.

Table 1. Composition of the column, clay, and micro-cellulose.

No. of Column	% of Clay	% of Micro-Cellulose	Filtering Time (h)
Column 1	100	0	1
Column 2	90	10	1.5
Column 3	80	20	2
Column 4	70	30	2.5
Column 5	60	40	3

2.3. Characterization

2.3.1. Thermogravimetric Analysis (TGA)

Thermogravimetry (TG) and differential thermogravimetry (DTG) techniques were employed to analyze the thermal stability of okra fibers. Analysis of the okra fiber was conducted using a thermogravimetric analyzer (Seiko, Tokyo, Japan, Model: Seiko Extar TG/DTSA-6300) to measure the weight loss of a sample as a function of temperature. In the TGA set-up, the fiber was heated at 20 °C/min. For all of the TGA experiments, 5 mg of fiber, a peak heating temperature of 600 °C, 10 min holding time, and N₂ gas flow rate 100 mL/min were used.

2.3.2. FTIR Spectroscopy

The FTIR measurements were carried out on a Shimadzu IR Prestige-21 Fourier Transform Infrared Spectrometer (Kyoto, Japan) to establish the functional group of the okra fiber and modified fiber with MCC. These samples were analyzed using solid-state Fourier transform infrared (FTIR) spectroscopy analysis on a Spectrum by a spectrometer. This was armed with a universal attenuated total reflection (ATR) sampling accessory and a scan range of 400–4000 cm⁻¹.

2.3.3. SEM Analysis

Morphological analysis of the surface of the produced MCC–clay composites, okra fiber, and clay was conducted using a JSM-6490 F model SEM machine manufactured by JEOL (Peabody, MA, USA).

2.3.4. XRD Analysis

XRD analysis of the pure fibers, clay, and composites was undertaken to find the crystallinity, which was carried out at room temperature with a D-8 ADVANCE Bruker diffractometer operating at 40 kV and 30 mA, using radiation ($\lambda = 0.1546$ nm) in a 2θ range of 5–35° at a scan rate of 4° min⁻¹. The crystallinity (X_c) values of these specimens were estimated from these X-ray diffraction measurements using Equation (1) [71]:

$$X_c(\%) = 100 \times \frac{S_c}{S_a + S_c} \quad (1)$$

where S_c and S_a are the crystalline and amorphous diffraction peak areas, respectively. The percentage of crystallinity (X_c) was calculated by a paper-cutting method using the paper weight of the respective areas, which is described in the Supplementary Materials (Figure S1) [71].

2.3.5. Metal Analysis by AAS

The Cu and Ni contents of the samples were analyzed by the atomic absorption spectrophotometric (Model-SpectrAA-220, Varian, Belrose, NSW, Australia) method [72]. First, the calibration curve was established using the working standard solutions from different concentrations of the certified reference material (CRM). The Cu and Ni contents

were measured using a direct flame method (air acetylene) at the wavelength of 327.4 and 232.0 nm, respectively. The efficiency of the okra MCC and clay composite for removing Cu^{+2} and Ni^{+2} from aqueous solutions was calculated quantitatively via Equation (2):

$$\text{Removal efficiency (\%)} = 100 \times \frac{C_i - C_f}{C_i} \quad (2)$$

where C_i is the initial metal ion concentration (mg/L) and C_f is the final (residual) metal ion concentration (mg/L). All determinations of Cu^{+2} and Ni^{+2} ions in the solution were carried out in triplicate.

2.3.6. Dye Absorbance Analysis by UV-Vis Spectrophotometer

UV analysis was carried out by a Shimadzu UV-1601 PC UV-Visible double beam spectrophotometer at a 190–1100 nm wavelength range. This served to find the absorbance capacity of the dye.

3. Result and Discussion

3.1. Okra Fiber and MCC Analysis

3.1.1. Thermogravimetric Analysis

Differential thermal analysis or DTA shows the phase change or melting point of a component. Figure 3 shows that the thermal degradation of MCC was greater than that of the raw fiber. This was due to the micro size and the larger number of the free end of the chain of MCC, which decomposes at a lower temperature. Sulfuric acid facilitates the decomposition of cellulose by removing some of the $-\text{OH}$ groups either by direct analysis or esterification [44]. Thermogravimetric analysis or TG% shows the change in mass over time. Pure cellulose has less TG% than raw okra fiber. Raw fiber has more mass change due to having more of the other constituents such as lignin, hemicellulose, and other non-cellulosic materials. The TG curve of okra fibers shows three weight loss steps, whilst their decomposition occurs in two main stages. The initial weight loss (6%) observed between 30 and 110 °C can be attributed to the vaporization of water from the fibers, while the onset degradation for the okra fibers occurred at a higher temperature, precisely after 250 °C. Above this temperature, it can be seen that the thermal stability gradually decreased, and degradation of the okra fibers occurred [44].

The first stage (250–310 °C) is associated with the thermal depolymerization of hemicellulose, pectin, and the cleavage of glycosidic linkages of cellulose, while the second one occurs in the range 310–390 °C and corresponds to the degradation of α -cellulose present in the fiber (weight loss 64.6%) [73]. Generally, the decomposition of lignin, due to its complex structure, occurs slowly within the whole temperature range. In fact, the lignin is composed of aromatic rings with various branches [74]. In MCC, all the hemicellulose, lignin, pectin materials are removed, leaving behind only cellulose, which shows a drastic change in weight loss at the initial stage [75]. Raw okra fiber has lignin, hemicellulose, and other non-cellulosic materials that show moisture loss in a wider range of temperature, while purified cellulose (Figure 3) is involved in relatively uniform sorptive forces, causing the loss of moisture within a narrow temperature change. In the case of MCC, sulfuric acid behaves as a dehydrating agent and sulfated groups reduce the affinity toward moisture absorption. The small quantity of moisture absorbed on the surface on MCC, and at a much lower temperature, it evaporated off from the surface [44].

3.1.2. FTIR of Different Okra Fiber

The peaks in the region 3600–3100 cm^{-1} corresponded to the characteristic O–H stretching vibration and hydrogen bond of the hydroxyl groups, which were observed in all spectra [76]. A vibration at 2980 cm^{-1} associated with C–H stretching vibrations was only found in the MCC spectra, which was for crystalline cellulose [77]. The shoulder, centered at 1602.85 cm^{-1} in the spectrum of raw okra fiber, can be attributed to the C=O

stretching of the acetyl and uronic ester groups of hemicellulose or the ester linkage of the carboxylic group of the ferulic and p-coumaric acids of lignin and/or hemicellulose [38,78], which disappeared after alkali treatment and bleaching (Figure 4). The peaks in the region between 1650 cm^{-1} and 1630 cm^{-1} were attributed to the adsorbed water [79]. The peaks of raw okra fiber at 1580 cm^{-1} were assigned to the skeleton vibration of C=C at an aromatic ring of lignin, which disappeared in the alkali-treated and bleached fiber, indicating the removal of lignin after chemical treatment [80]. The C=C stretching from the aromatic ring of the lignin showed peaks at 1508 cm^{-1} and C–O–C (aryl-alkyl ether) at 1247 cm^{-1} in the spectra of the raw fiber and alkali-treated fiber. These two peaks decreased in the spectrum of the fibers after bleaching [78,81], which strongly suggests that bleaching is an effective way to remove lignin. In the spectrum of cellulose whiskers, no difference was found compared with that of the extracted cellulose.

Thus, in the case of hydrolysis, the molecular structure of cellulose did not change [35,39]. Another two peaks around 1060 cm^{-1} and 895 cm^{-1} were found in all of the spectra and were associated with the C–O stretching and C–H rocking vibrations, which means that cellulose was present [38]. In all of the spectra, we saw no change in the cellulose composition, which means that no chemical change occurred during various chemical treatments for cellulose. In fact, only non-cellulosic substances such as lignin, hemicellulose, and other dirt materials were removed.

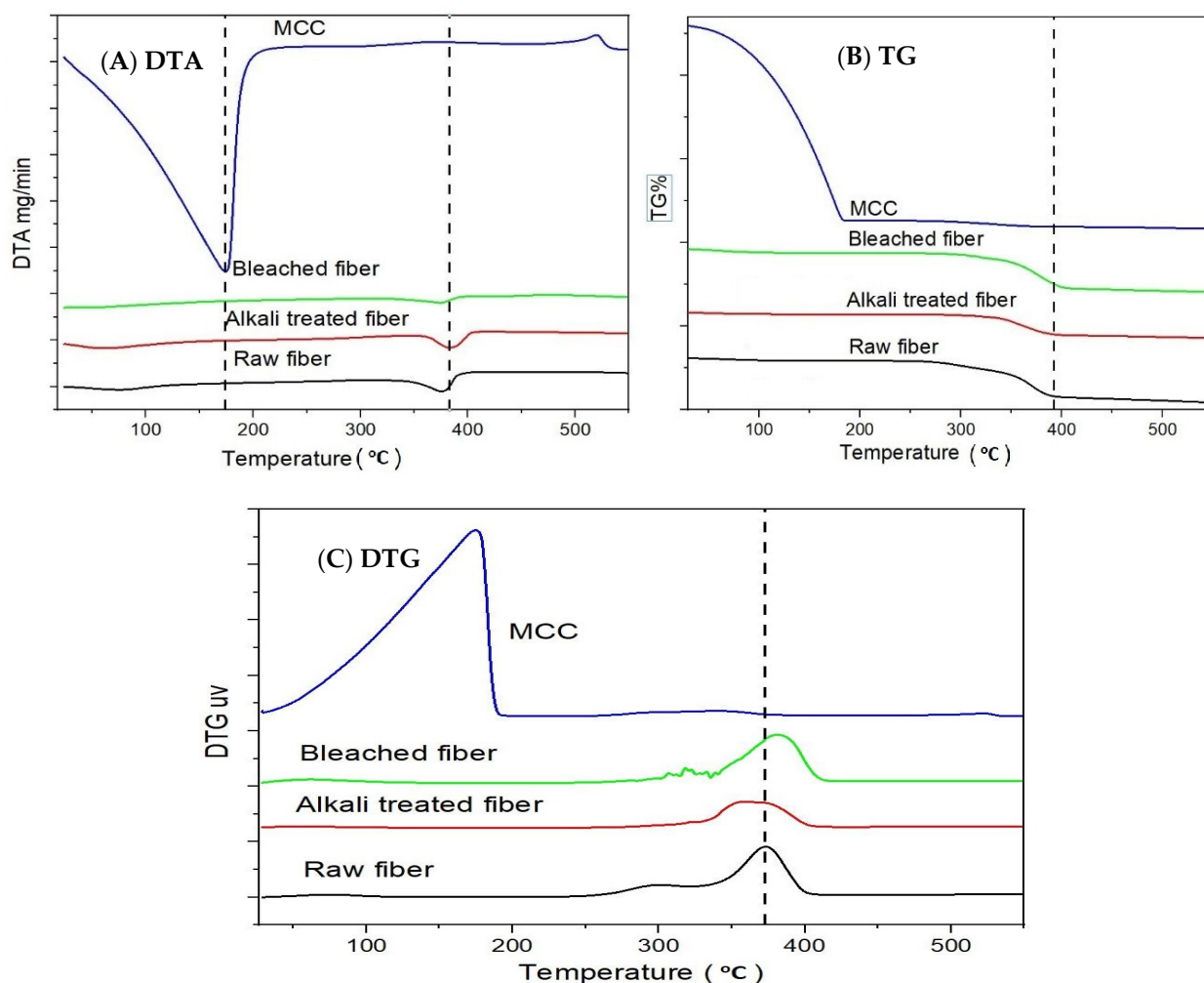


Figure 3. Thermogravimetric ((A) DTA, (B) TG, and (C) DTG) profiles of the raw, alkali treated, bleached fiber, and microcrystalline cellulose (MCC).

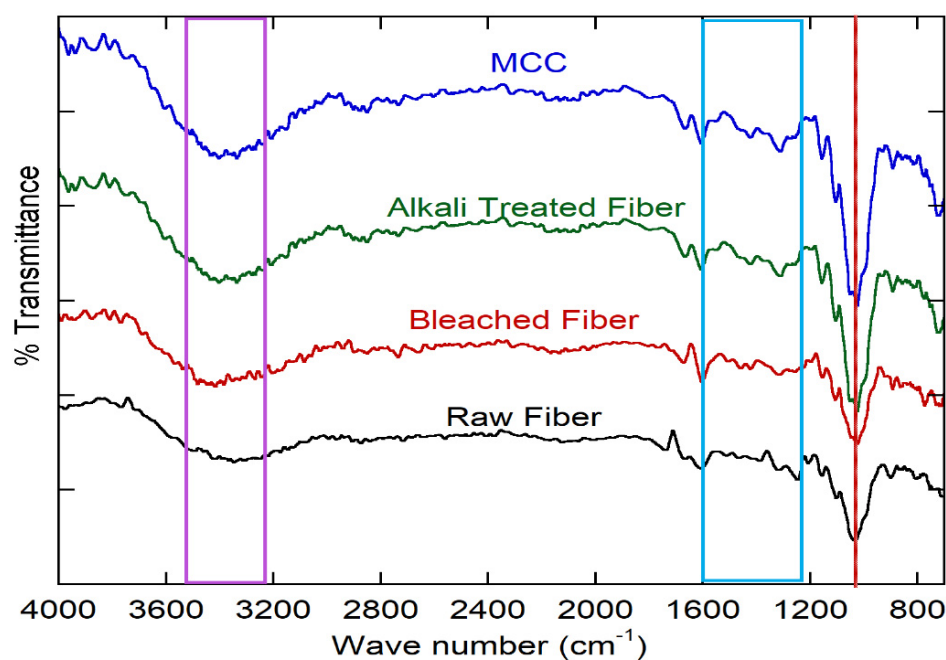


Figure 4. FTIR spectra of the raw, alkali treated, bleached fiber, and microcrystalline cellulose (MCC).

3.1.3. XRD Analysis

Figure 5 shows the XRD spectra of the raw fiber, alkali treated fiber, bleached fiber, and microcrystalline cellulose (MCC). From the spectra, it can be seen that a broad peak in $2\theta = 20\text{--}25^\circ$ became sharper from the raw fiber to MCC. This indicates the presence of cellulose and the sharp peak reflects the increasing portion of the crystalline structure of cellulose. The crystallinity of the raw fiber, alkali treated fiber, bleached fiber, and MCC were 40.54%, 55.26%, 65.84%, and 81.08%, respectively. This indicates that there was no change in cellulose during the chemical treatment, however, only the crystallinity was increased. The crystallinity was increased undoubtedly due to the removal of hemicellulose and lignin, which exist in amorphous regions. This leads to the realignment of cellulose molecules to a more crystalline structure in MCC and supports the reported results [38]. The raw fiber showed diffraction peaks at around $2\theta = 16.2^\circ$ and 22.3° , which corresponded to the (101) and (002) planes, respectively, which is for the cellulose I structure. Additionally, the peak at around $2\theta = 16.2^\circ$ may have a combination of two peaks, highlighting the presence of a small amount of cellulose II structure [82]. The spectrum of MCC also showed a new peak at around $2\theta = 12.36^\circ$, which was indexed for the plane (110), revealing the presence of cellulose II crystallites [43].

3.1.4. SEM Analysis

Figure 6A–D presents the SEM photographs of the raw, bleached, alkali, and acid-treated okra fibers, respectively. In Figure 6A, it appears that the fiber contained fatty and waxy materials, lignin, hemicellulose, and other impurities. Figure 6B shows that fatty and waxy materials, lignin, and other impurities were mostly removed after bleaching treatment. Figure 6C confirms that hemicellulose was removed after alkali treatment, which decreased the fiber's diameter. After treatment with H_2SO_4 , the cellulose fibers were separated into individual micro-sized fibers (Figure 6D). In fact, these micro-sized fibers were reportedly composed of strong hydrogen bonding nanofibers, and individualized nanofiber bundles with a width of 300 nm to several micrometers can be seen on the surface of the micro-sized cellulose fiber (Figure 6D). These support the reported results [48,65].

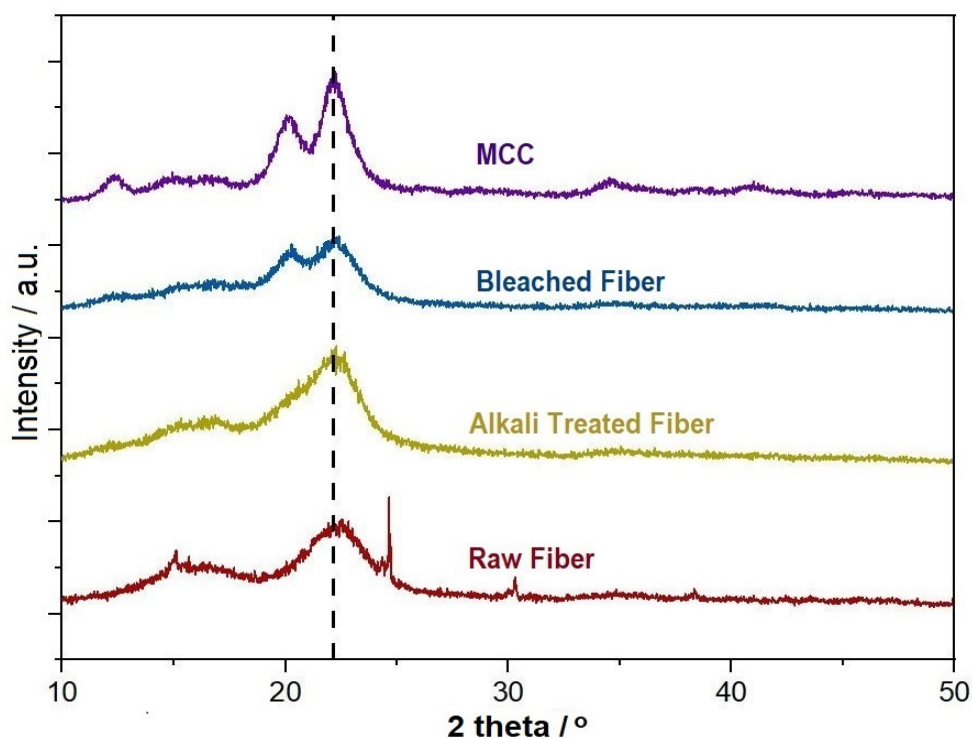


Figure 5. XRD spectra of the raw, alkali treated, bleached fiber, and microcrystalline cellulose (MCC).

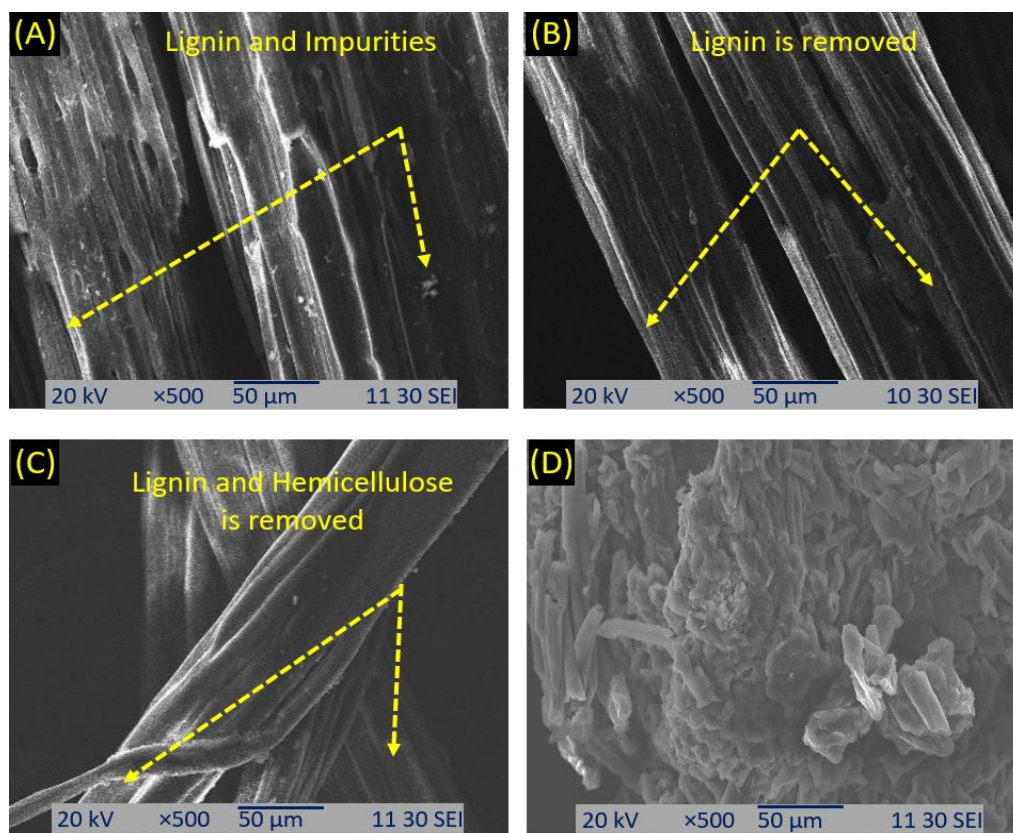


Figure 6. SEM photographs of the raw (A), alkali treated (B), bleached fiber (C), and microcrystalline cellulose (MCC) (D).

3.2. Characterization of Clay

3.2.1. SEM Analysis of Clay

A topographical and morphological evaluation of clay materials was carried out by SEM examination of the samples. Close examination of these images revealed that the clay materials did not display any particular morphology; instead, they indicated the presence of small crystallites of dissimilar sizes [54]. Figure 7A,B shows the SEM analysis of untreated clay, where the surface of the clay was very smooth. Figure 7C,D reveals that after the treatment of clay, the surface became very rough.

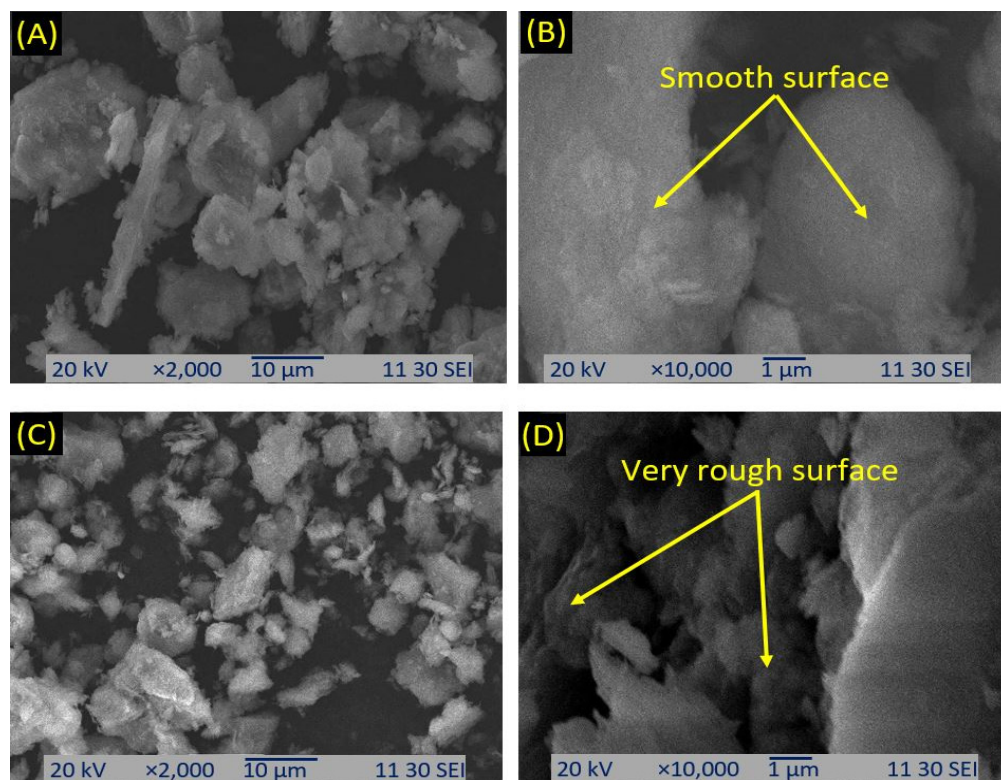


Figure 7. SEM photographs of the raw (A,B) and modified clay (C,D) with different magnifications.

3.2.2. XRD Analysis of Clay

Figure 8 presents the XRD profiles of the untreated and treated clay. From this figure, it was revealed that the two profiles showed similar peaks of 'K' and 'Q', where 'K' stands for 'Kaolinite' and 'Q' stands for 'Quartz'. There was no change in the chemical composition after treatment by ethylene diamine. The peaks at the 2θ value of 26.6 was attributed to the presence of the quartz mineral and support the reported results [54]. After treatment, impurities dissolved and hydrophobicity was increased. Analysis of the XRD data showed that Bijoypur clay is mainly a kaolinite type of mineral (aluminum silicate hydroxide, $\text{Al}_2\text{Si}_2\text{O}_5(\text{OH})_4$). However, the X-ray data did indicate small amounts of quartz (silicon oxide, SiO_2) and trace amounts of chlorite (sodium aluminum silicate hydroxide hydrate, $\text{Na}_2\text{O} \cdot \text{Al}_2\text{O}_3 \cdot \text{SiO}_2(\text{OH})_4 \cdot x\text{H}_2\text{O}$) and illite (potassium aluminum silicate hydroxide, $\text{KAl}_2\text{Si}_3\text{AlO}_{10}(\text{OH})_2$) present in the clay samples. Some weak lines of chlorite and illite were not observed in the X-ray films, which may be due to the fact that the amount of chlorite and illite is minute in the local clay [54].

3.3. Characterization of Column

3.3.1. Metal Analysis by AAS

From Figure 9, it can be seen that the amounts of copper (Cu) and nickel (Ni) removal in water as the percentage of MCC increased in the column. Filter 1 contained 100% of

clay while Filter 2 contained 90% clay and 10% MCC. Filter 3 contained 80% clay and 20% MCC. Filter 4 contained 70% clay and 30% MCC. Filter 5 contained 60% clay and 40% MCC. Therefore, it was observed that both clay and MCC had more absorption capacity. However, MCC had more absorption capacity than clay. This absorption also increased continuously until the ideal limit was reached, which is 30% MCC. After that, the absorption capacity declined. The MCC contains very fine pores and after using more than 30%, the wastewater takes more time to pass through it. Moreover, both clay and MCC were enhanced to absorb the metal molecule. As the amount of clay decreased, the absorption increased until a certain point was reached. After reducing the amount of clay, the absorption of metal molecules will decrease. Therefore, the percentage that obtained a minimum value of Cu (0.07 mg/ L) was 30% of MCC and 70% of clay. The maximum adsorption of Cu and Ni, which were almost 94% and 100%, respectively, were observed in Filter 4, containing 70% clay and 30% MCC. The maximum Cu removal efficiency was reported as 30 mg/g at pH 5 using dolochar; 0.04 mg/g using the polyhydroquinone/graphene nanocomposite, and 96.33% at pH 5 in past studies [83–85]. Bartzak et al. [86] reported a higher Ni sorption of 61.27 mg/L by peat at pH 4. In a recent study, Al-Abbad et al. [87] used Jordanian natural zeolite, which had a high Ni removal capacity of 153.85 mg/g with a 4 h contact time.

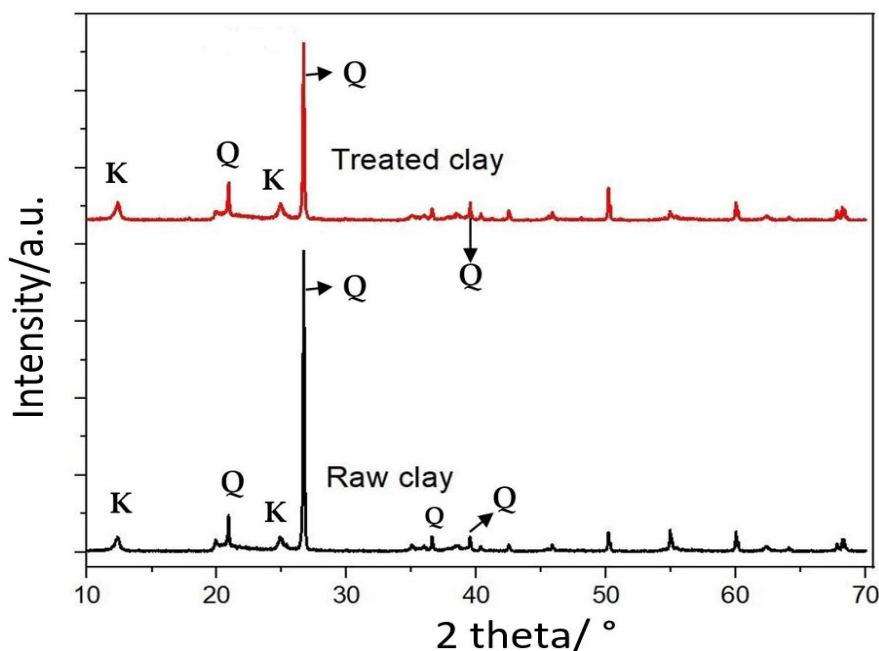


Figure 8. XRD analysis of the raw and treated clay.

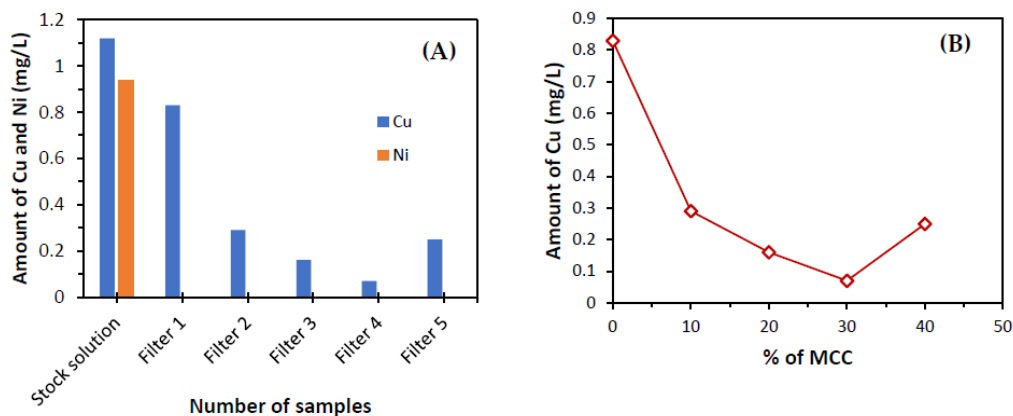


Figure 9. (A,B) Analysis of Cu and Ni by AAS.

3.3.2. Dye Absorbance Analysis by UV–Vis Spectrophotometer

The absorbance of the dye solution was 0.720 nm (520 nm range). Filter 1 contained 100% clay and its absorption value was 0.55. Filter 2 contained 90% clay and 10% MCC, and their absorption value was 0.45. Filter 3 contained 80% clay and 20% MCC, and their absorption value was 0.39. Filter 4 contained 70% clay and 30% MCC, and their absorption value was 0.29. Filter 5 contained 60% clay and 40% MCC, and their absorption value amounted to 0.11. The maximum absorbance of dye was observed in Filter 5 and was almost 85%. Looking at Figure 10B, the absorbance capacity decreased with the increase in MCC. Conversely, the absorption capacity of the dye molecules increased with the increased amount of clay. Both the nanocellulose and clay samples could enhance the absorption of dye molecules from wastewater, while the micro-cellulose could absorb dye molecules from the wastewater at a minimum quantity; adding clay increased the capacity of the absorbance of dye molecules from wastewater [88].

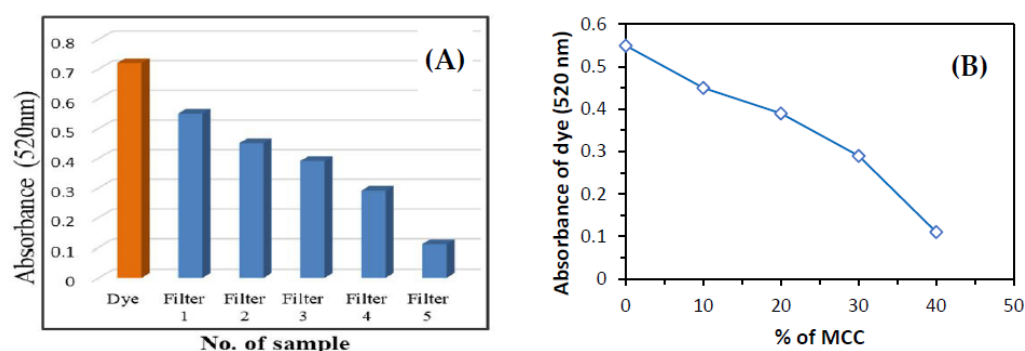


Figure 10. (A,B) UV analysis of dye.

3.3.3. XRD Analysis of Packing Columns

The curves indicated by packing columns 1, 2, 3, 4, and 5 are illustrated in Figure 11. Packing 1 was composed of 100% clay; packing 2 was composed of 90% clay and 10% MCC; packing 3 consisted of 80% clay and 20% MCC; packing 4 was made up of 70% clay and 30% MCC; packing 5 was composed of 60% clay and 40% MCC. In Figure 11, all the curves showed the same peaks of 'K' and 'Q', where 'K' stands for 'Kaolinite' and 'Q' stands for 'Quartz'. Based on the XRD analysis, it is evident that after the purification of water, no change in the chemical composition of clay occurred.

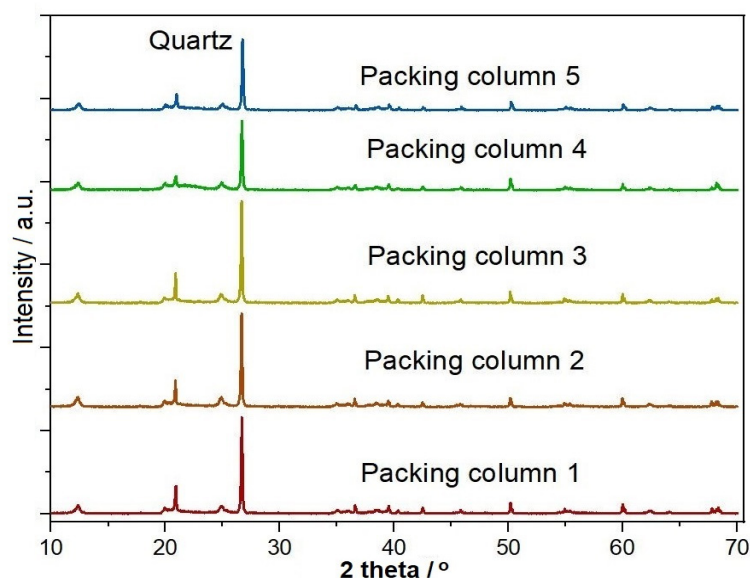


Figure 11. XRD analysis of the different packing columns.

3.3.4. SEM Analysis

Figure 12 represents the SEM micrograph of the 100% clay column. The 100% clay had a poorer absorption capacity of the dye and metal ions from the solution when compared to the other percentage-containing column. Here, no MCC was used, which can amplify the absorption capacity of clay.

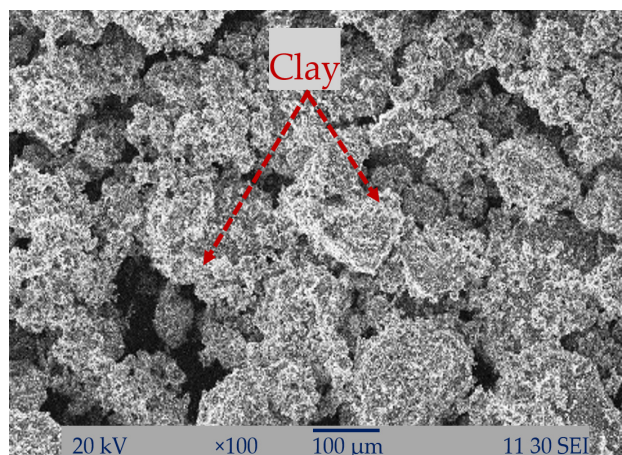


Figure 12. SEM analysis of the 100% clay packing column.

Figure 13 depicts the SEM analysis of the columns represented by A, B, C, and D, which were composed of 90% clay and 10% MCC, 80% clay and 20% MCC, 70% clay and 30% MCC, and 60% clay and 40% MCC, respectively. When MCC was incorporated into clay, its capacity to adsorb dye and metal ions was enhanced. This is because clay and MCC both have their own absorption capacities and when they are combined, clay amplifies the absorption capacity of MCC. However, for MCC, the absorption capacity is increased up to a certain limit for MCC (30%). After that, the absorption capacity diminishes with the filtration time due to the small pore size of MCC (300–600 nm), which was measured during the SEM analysis of MCC. This was observed as hindering the ability of water to pass through the filter.

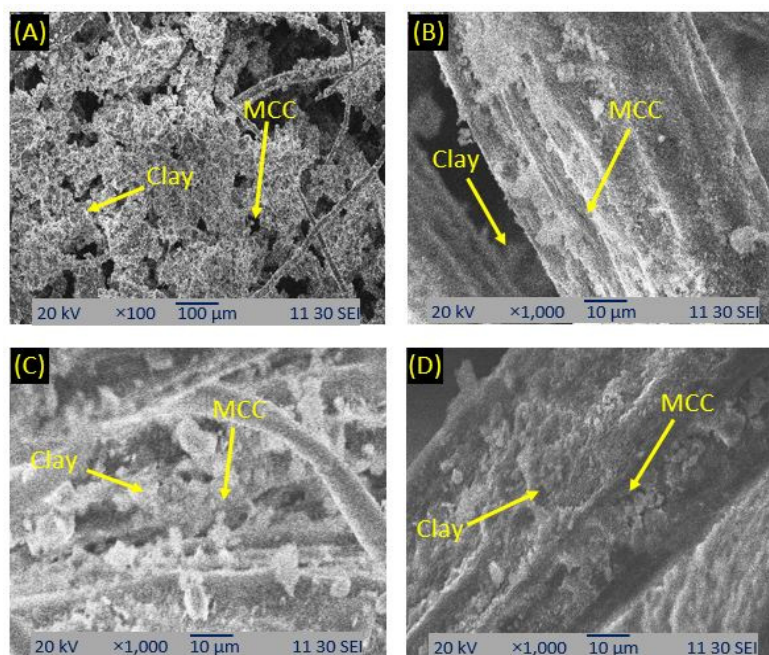


Figure 13. SEM analysis of packing column 1 (A), packing column 2 (B), packing column 3 (C), and packing column 4 (D).

4. Conclusions

Micro-composites were prepared by Okra MCC and treated micro-clay, then applied to remove Cu and Ni from wastewater. Both MCC and clay enhanced Cu, Ni and dye (basic yellow II) absorption capacity from wastewater. The efficiency of metal and dye absorption is up to 26% for Cu and 24% for dye (basic yellow II) when utilizing pure clay, whereas the efficiency of metal absorption is up to 95% for Cu and 100% for Ni by MCC and clay composite. UV visible absorption shows a remarkable result for the MCC and clay composite, which can absorb as much as 85% of basic yellow (II) dye from wastewater. As the percentage of MCC rises, the percentage of absorption of dye also increases. Further research is warranted to provide detailed and technical insights on the effect of a series of different columns on MCC's efficiency in removing Cu and Ni, in both mono and binary sorption (competitive) systems. It is imperative to explore what are the most efficient approaches to safely treat the Cu, Ni and dye residues of spent MCC after adsorption. This refers to the elemental desorption, bioleaching, and/or stabilization of Cu, Ni and dye-rich MCC.

Supplementary Materials: The following supporting information can be downloaded at: <https://www.mdpi.com/article/10.3390/reactions4030021/s1>, Figure S1: Determination of crystallinity (%) by paper cutting method using Sc and Sa.

Author Contributions: A.A.M.: Conceptualization, Data curation, Formal analysis, Methodology, Validation, Visualization, Writing—original draft, Writing—review & editing; M.A.R.: Methodology, Investigation, Validation, Visualization, Resources, Formal analysis, Writing—extensively review & editing, submission; M.H.R.: Methodology, Formal analysis, Validation, Writing—review & editing; M.M.: Conceptualization, Resources, Writing—review & editing; S.M.F.: Writing—review & editing; M.M.I.: Writing—review & editing; M.S.I.K.: Writing—review & editing; M.Z.P.: Writing—review & editing. All authors have read and agreed to the published version of the manuscript.

Funding: This research received no external funding.

Data Availability Statement: The data of this study will be shared upon reasonable request to the corresponding author.

Conflicts of Interest: The authors declare no conflict of interest.

References

1. Grey, D.; Garrick, D.; Blackmore, D.; Kelman, J.; Muller, M.; Sadoff, C. Water security in one blue planet: Twenty-first century policy challenges for science. *Philos. Trans. R. Soc. A Math. Phys. Eng. Sci.* **2013**, *371*, 20120406. [CrossRef]
2. Vörösmarty, C.J.; McIntyre, P.B.; Gessner, M.O.; Dudgeon, D.; Prusevich, A.; Green, P.; Glidden, S.; Bunn, S.E.; Sullivan, C.A.; Liermann, C.R. Global threats to human water security and river biodiversity. *Nature* **2010**, *467*, 555–561. [CrossRef]
3. Bakker, K. Water security: Research challenges and opportunities. *Science* **2012**, *337*, 914–915. [CrossRef] [PubMed]
4. Peralta-Videa, J.R.; Lopez, M.L.; Narayan, M.; Saupe, G.; Gardea-Torresdey, J. The biochemistry of environmental heavy metal uptake by plants: Implications for the food chain. *Int. J. Biochem. Cell Biol.* **2009**, *41*, 1665–1677. [CrossRef] [PubMed]
5. Sultana, M.; Rownok, M.H.; Sabrin, M.; Rahaman, M.H.; Alam, S.N. A review on experimental chemically modified activated carbon to enhance dye and heavy metals adsorption. *Clean. Eng. Technol.* **2022**, *6*, 100382. [CrossRef]
6. Alloway, B.J. Sources of heavy metals and metalloids in soils. In *Heavy Metals in Soils*; Springer: Berlin/Heidelberg, Germany, 2013; pp. 11–50.
7. Ali, I. New generation adsorbents for water treatment. *Chem. Rev.* **2012**, *112*, 5073–5091. [CrossRef] [PubMed]
8. Sholl, D.S.; Lively, R.P. Seven chemical separations to change the world. *Nature* **2016**, *532*, 435–437. [CrossRef]
9. Sujatha, S.; Rajamohan, N.; Anbazhagan, S.; Vanithasri, M.; Rajasimman, M. Extraction of nickel using a green emulsion liquid membrane—Process intensification, parameter optimization and artificial neural network modeling. *Chem. Eng. Process-Process Intensif.* **2021**, *165*, 108444. [CrossRef]
10. Hashem, M.A.; Nur-A-Tomal, M.S.; Mondal, N.R.; Rahman, M.A. Hair burning and liming in tanneries is a source of pollution by arsenic, lead, zinc, manganese and iron. *Environ. Chem. Lett.* **2017**, *15*, 501–506. [CrossRef]
11. Rahman, A.; Rahaman, H. Contamination of arsenic, manganese and coliform bacteria in groundwater at Kushtia District, Bangladesh: Human health vulnerabilities. *J. Water Health* **2018**, *16*, 782–795. [CrossRef]
12. Talukdar, M.; Hasnine, M. Application of Chitosan-Based Filtration Technique for Removal of Heavy Metals from Surface Water. *Int. Res. J. Environ. Sci.* **2014**, *3*, 5–10.

13. WHO. *World Health Organization. Guidelines for Drinking-Water Quality*, 4th ed.; World Health Organization: Geneva, Switzerland, 2011.
14. ECR. *Environment Conservation Rules*; Department of Environment & Forest Ministry, Government of Bangladesh: Dhaka, Bangladesh, 1997; pp. 206–207.
15. Hernández-Hernández, K.; Illescas, J.; Díaz-Nava, M.; Muro-Urista, C.; Martínez-Gallegos, S.; Ortega-Aguilar, R. Polymer-clay nanocomposites and composites: Structures, characteristics, and their applications in the removal of organic compounds of environmental interest. *Med. Chem* **2016**, *6*, 201–210. [[CrossRef](#)]
16. Rahman, M.A.; Lamb, D.; Rahman, M.M.; Bahar, M.M.; Sanderson, P.; Abbasi, S.; Bari, A.F.; Naidu, R. Removal of arsenate from contaminated waters by novel zirconium and zirconium-iron modified biochar. *J. Hazard. Mater.* **2021**, *409*, 124488. [[CrossRef](#)] [[PubMed](#)]
17. Rahman, M.A.; Lamb, D.; Rahman, M.M.; Bahar, M.M.; Sanderson, P. Adsorption–Desorption Behavior of Arsenate Using Single and Binary Iron-Modified Biochars: Thermodynamics and Redox Transformation. *ACS Omega* **2022**, *7*, 101–117. [[CrossRef](#)]
18. Huang, N.; Zhai, L.; Xu, H.; Jiang, D. Stable covalent organic frameworks for exceptional mercury removal from aqueous solutions. *J. Am. Chem. Soc.* **2017**, *139*, 2428–2434. [[CrossRef](#)]
19. Li, B.; Zhang, Y.; Ma, D.; Shi, Z.; Ma, S. Mercury nano-trap for effective and efficient removal of mercury (II) from aqueous solution. *Nat. Commun.* **2014**, *5*, 1–7. [[CrossRef](#)]
20. Vilela, D.; Parmar, J.; Zeng, Y.; Zhao, Y.; Sánchez, S. Graphene-based microbots for toxic heavy metal removal and recovery from water. *Nano Lett.* **2016**, *16*, 2860–2866. [[CrossRef](#)]
21. Rahaman, M.H.; Islam, M.A.; Islam, M.M.; Rahman, M.A.; Alam, S.N. Biodegradable composite adsorbent of modified cellulose and chitosan to remove heavy metal ions from aqueous solution. *Curr. Res. Green Sustain. Chem.* **2021**, *4*, 100119. [[CrossRef](#)]
22. Berslin, D.; Reshmi, A.; Sivaprakash, B.; Rajamohan, N.; Kumar, P.S. Remediation of emerging metal pollutants using environment friendly biochar-Review on applications and mechanism. *Chemosphere* **2022**, *290*, 133384. [[CrossRef](#)]
23. Kołodziejka, D.; Krukowska, J.; Thomas, P. Comparison of sorption and desorption studies of heavy metal ions from biochar and commercial active carbon. *Chem. Eng. J.* **2017**, *307*, 353–363. [[CrossRef](#)]
24. Seliman, A.; Lasheen, Y.; Youssief, M.; Abo-Aly, M.; Shehata, F. Removal of some radionuclides from contaminated solution using natural clay: Bentonite. *J. Radioanal. Nucl. Chem.* **2014**, *300*, 969–979. [[CrossRef](#)]
25. Lu, X.; Wang, F.; Li, X.-Y.; Shih, K.; Zeng, E.Y. Adsorption and thermal stabilization of Pb²⁺ and Cu²⁺ by zeolite. *Ind. Eng. Chem. Res.* **2016**, *55*, 8767–8773. [[CrossRef](#)]
26. Mon, M.; Ferrando-Soria, J.; Grancha, T.; Fortea-Perez, F.R.; Gascon, J.; Leyva-Perez, A.; Armentano, D.; Pardo, E. Selective gold recovery and catalysis in a highly flexible methionine-decorated metal–organic framework. *J. Am. Chem. Soc.* **2016**, *138*, 7864–7867. [[CrossRef](#)]
27. Sun, Q.; Aguila, B.; Perman, J.; Earl, L.D.; Abney, C.W.; Cheng, Y.; Wei, H.; Nguyen, N.; Wojtas, L.; Ma, S. Postsynthetically modified covalent organic frameworks for efficient and effective mercury removal. *J. Am. Chem. Soc.* **2017**, *139*, 2786–2793. [[CrossRef](#)] [[PubMed](#)]
28. Chakraborty, A.; Bhattacharyya, S.; Hazra, A.; Ghosh, A.C.; Maji, T.K. Post-synthetic metalation in an anionic MOF for efficient catalytic activity and removal of heavy metal ions from aqueous solution. *Chem. Commun.* **2016**, *52*, 2831–2834. [[CrossRef](#)]
29. Aguila, B.; Sun, Q.; Perman, J.A.; Earl, L.D.; Abney, C.W.; Elzein, R.; Schlaf, R.; Ma, S. Efficient mercury capture using functionalized porous organic polymer. *Adv. Mater.* **2017**, *29*, 1700665. [[CrossRef](#)] [[PubMed](#)]
30. Fratzl, P. Biomimetic materials research: What can we really learn from nature’s structural materials? *J. R. Soc. Interface* **2007**, *4*, 637–642. [[CrossRef](#)]
31. Wicklein, B.; Salazar-Alvarez, G. Functional hybrids based on biogenic nanofibrils and inorganic nanomaterials. *J. Mater. Chem. A* **2013**, *1*, 5469–5478. [[CrossRef](#)]
32. Nechyporchuk, O.; Belgacem, M.N.; Bras, J. Production of cellulose nanofibrils: A review of recent advances. *Ind. Crops Prod.* **2016**, *93*, 2–25. [[CrossRef](#)]
33. Sticklen, M.B. Plant genetic engineering for biofuel production: Towards affordable cellulosic ethanol. *Nat. Rev. Genet.* **2008**, *9*, 433–443. [[CrossRef](#)]
34. Abe, K.; Iwamoto, S.; Yano, H. Obtaining cellulose nanofibers with a uniform width of 15 nm from wood. *Biomacromolecules* **2007**, *8*, 3276–3278. [[CrossRef](#)]
35. Chen, Y.; Liu, C.; Chang, P.R.; Cao, X.; Anderson, D.P. Bionanocomposites based on pea starch and cellulose nanowhiskers hydrolyzed from pea hull fibre: Effect of hydrolysis time. *Carbohydr. Polym.* **2009**, *76*, 607–615. [[CrossRef](#)]
36. Abe, K.; Yano, H. Comparison of the characteristics of cellulose microfibril aggregates isolated from fiber and parenchyma cells of Moso bamboo (*Phyllostachys pubescens*). *Cellulose* **2010**, *17*, 271–277. [[CrossRef](#)]
37. Morán, J.I.; Alvarez, V.A.; Cyras, V.P.; Vázquez, A. Extraction of cellulose and preparation of nanocellulose from sisal fibers. *Cellulose* **2008**, *15*, 149–159. [[CrossRef](#)]
38. Alemdar, A.; Sain, M. Isolation and characterization of nanofibers from agricultural residues–Wheat straw and soy hulls. *Bioresour. Technol.* **2008**, *99*, 1664–1671. [[CrossRef](#)]
39. Li, R.; Fei, J.; Cai, Y.; Li, Y.; Feng, J.; Yao, J. Cellulose whiskers extracted from mulberry: A novel biomass production. *Carbohydr. Polym.* **2009**, *76*, 94–99. [[CrossRef](#)]

40. de Morais Teixeira, E.; Corrêa, A.C.; Manzoli, A.; de Lima Leite, F.; de Oliveira, C.R.; Mattoso, L.H.C. Cellulose nanofibers from white and naturally colored cotton fibers. *Cellulose* **2010**, *17*, 595–606. [[CrossRef](#)]
41. Wang, B.; Sain, M.; Oksman, K. Study of structural morphology of hemp fiber from the micro to the nanoscale. *Appl. Compos. Mater.* **2007**, *14*, 89–103. [[CrossRef](#)]
42. Rosa, M.; Medeiros, E.; Malmonge, J.; Gregorski, K.; Wood, D.; Mattoso, L.; Glenn, G.; Orts, W.; Imam, S. Cellulose nanowhiskers from coconut husk fibers: Effect of preparation conditions on their thermal and morphological behavior. *Carbohydr. Polym.* **2010**, *81*, 83–92. [[CrossRef](#)]
43. Zuluaga, R.; Putaux, J.L.; Cruz, J.; Vélez, J.; Mondragon, I.; Gañán, P. Cellulose microfibrils from banana rachis: Effect of alkaline treatments on structural and morphological features. *Carbohydr. Polym.* **2009**, *76*, 51–59. [[CrossRef](#)]
44. De Rosa, I.M.; Kenny, J.M.; Puglia, D.; Santulli, C.; Sarasini, F. Morphological, thermal and mechanical characterization of okra (*Abelmoschus esculentus*) fibres as potential reinforcement in polymer composites. *Compos. Sci. Technol.* **2010**, *70*, 116–122. [[CrossRef](#)]
45. Dinand, E.; Chanzy, H.; Vignon, R. Suspensions of cellulose microfibrils from sugar beet pulp. *Food Hydrocoll.* **1999**, *13*, 275–283. [[CrossRef](#)]
46. Jiang, F.; Kondo, T.; Hsieh, Y.-L. Rice straw cellulose nanofibrils via aqueous counter collision and differential centrifugation and their self-assembled structures. *ACS Sustain. Chem. Eng.* **2016**, *4*, 1697–1706. [[CrossRef](#)]
47. Kang, X.; Sun, P.; Kuga, S.; Wang, C.; Zhao, Y.; Wu, M.; Huang, Y. Thin cellulose nanofiber from corn cob cellulose and its performance in transparent nanopaper. *ACS Sustain. Chem. Eng.* **2017**, *5*, 2529–2534. [[CrossRef](#)]
48. Amiralian, N.; Annamalai, P.K.; Memmott, P.; Taran, E.; Schmidt, S.; Martin, D.J. Easily deconstructed, high aspect ratio cellulose nanofibres from *Triodia pungens*; an abundant grass of Australia's arid zone. *RSC Adv.* **2015**, *5*, 32124–32132. [[CrossRef](#)]
49. Voisin, H.; Bergström, L.; Liu, P.; Mathew, A.P. Nanocellulose-based materials for water purification. *Nanomaterials* **2017**, *7*, 57. [[CrossRef](#)]
50. Sheltami, R.M.E.; Abdullah, I.; Ahmad, I. Structural Characterisation of Cellulose and Nanocellulose Extracted from Mengkuang Leaves. *Adv. Mater. Res.* **2012**, *545*, 119–123. [[CrossRef](#)]
51. Wolfe, T.A.; Demirel, T.; Baumann, E.R. Adsorption of organic pollutants on montmorillonite treated with amines. *J. Water Pollut. Control Fed.* **1986**, *58*, 68–76.
52. Luh, M.-D.; Baker, R.A. Vapor phase sorption of phenol on selected clays. *J. Colloid Interface Sci.* **1970**, *33*, 539–547. [[CrossRef](#)]
53. Oliveira, L.C.; Rios, R.V.; Fabris, J.D.; Sapag, K.; Garg, V.K.; Lago, R.M. Clay-iron oxide magnetic composites for the adsorption of contaminants in water. *Appl. Clay Sci.* **2003**, *22*, 169–177. [[CrossRef](#)]
54. Miran, M.; Mollah, M.; Hussain, A.; Rahman, M. A multi-technique characterization of Bijoypur clay. *Bangladesh J. Sci. Res.* **2008**, *21*, 2.
55. Varga, G. The structure of kaolinite and metakaolinite. *Epitoanyag* **2007**, *59*, 6–9. [[CrossRef](#)]
56. Madejová, J. FTIR techniques in clay mineral studies. *Vib. Spectrosc.* **2003**, *31*, 1–10. [[CrossRef](#)]
57. Ci, Z.; Yue, Y.; Xiao, J.; Huang, X.; Sun, Y. Spectroscopic and modeling investigation of U (VI) removal mechanism on nanoscale zero-valent iron/clay composites. *J. Colloid Interface Sci.* **2023**, *630*, 395–403. [[CrossRef](#)] [[PubMed](#)]
58. Ghasemi, H.; Afshang, M.; Gilvari, T.; Aghabarari, B.; Mozaffari, S. Rapid and effective removal of heavy metal ions from aqueous solution using nanostructured clay particles. *Results Surf. Interfaces* **2023**, 100097. [[CrossRef](#)]
59. Sjöberg, M.; Bergström, L.; Larsson, A.; Sjöström, E. The effect of polymer and surfactant adsorption on the colloidal stability and rheology of kaolin dispersions. *Colloids Surf. A Physicochem. Eng. Asp.* **1999**, *159*, 197–208. [[CrossRef](#)]
60. Lin, S.-H.; Juang, R.-S. Heavy metal removal from water by sorption using surfactant-modified montmorillonite. *J. Hazard. Mater.* **2002**, *92*, 315–326. [[CrossRef](#)]
61. Mu, B.; Wang, A. One-pot fabrication of multifunctional superparamagnetic attapulgite/Fe₃O₄/polyaniline nanocomposites served as an adsorbent and catalyst support. *J. Mater. Chem. A* **2015**, *3*, 281–289. [[CrossRef](#)]
62. Yang, S.; Ren, X.; Zhao, G.; Shi, W.; Montavon, G.; Grambow, B.; Wang, X. RETRACTED: Competitive sorption and selective sequence of Cu (II) and Ni (II) on montmorillonite: Batch, modeling, EPR and XAS studies. *Geochim. Cosmochim. Acta* **2015**, *166*, 129–145. [[CrossRef](#)]
63. Yang, S.; Okada, N.; Nagatsu, M. The highly effective removal of Cs⁺ by low turbidity chitosan-grafted magnetic bentonite. *J. Hazard. Mater.* **2016**, *301*, 8–16. [[CrossRef](#)]
64. Maniruzzaman, M.; Rahman, M.; Zaman, M. Composition of agave atrovérance fiber. *Jahangirnagar Univ. J. Sci.* **2005**, *28*, 23–30.
65. Sarkar, P.; Mazumdar, A.; Pal, K. 4—The hemicelluloses of jute fibre. *J. Text. Inst. Trans.* **1948**, *39*, T44–T58. [[CrossRef](#)]
66. Nascimento, D.M.; Nunes, Y.L.; Figueirêdo, M.C.; de Azeredo, H.M.; Aouada, F.A.; Feitosa, J.P.; Rosa, M.F.; Dufresne, A. Nanocellulose nanocomposite hydrogels: Technological and environmental issues. *Green Chem.* **2018**, *20*, 2428–2448. [[CrossRef](#)]
67. Yang, J.; Han, C.-R.; Duan, J.-F.; Ma, M.-G.; Zhang, X.-M.; Xu, F.; Sun, R.-C.; Xie, X.-M. Studies on the properties and formation mechanism of flexible nanocomposite hydrogels from cellulose nanocrystals and poly (acrylic acid). *J. Mater. Chem.* **2012**, *22*, 22467–22480. [[CrossRef](#)]
68. Rahaman, M.H.; Haque, M.A.; Rahman, M.A.; Rana, M.M.; Parvez, M.M.; Alam, S.N. Grafting of Cellulose and Microcrystalline Cellulose with Oligo (L-lactic acid) by Polycondensation Reaction. *Reactions* **2022**, *3*, 213–223. [[CrossRef](#)]
69. Islam, M.M.; Khan, M.N.; Biswas, S.; Choudhury, T.R.; Haque, P.; Rashid, T.U.; Rahman, M.M. Preparation and characterization of bijoypur clay-crystalline cellulose composite for application as an adsorbent. *Adv. Mater. Sci* **2017**, *2*, 1–7. [[CrossRef](#)]

70. Gabr, M.H.; Phong, N.T.; Abdelkareem, M.A.; Okubo, K.; Uzawa, K.; Kimpara, I.; Fujii, T. Mechanical, thermal, and moisture absorption properties of nano-clay reinforced nano-cellulose biocomposites. *Cellulose* **2013**, *20*, 819–826. [[CrossRef](#)]
71. Rahaman, M.H.; Tsuji, H. Isothermal crystallization and spherulite growth behavior of stereo multiblock poly (lactic acid) s: Effects of block length. *J. Appl. Polym. Sci.* **2013**, *129*, 2502–2517. [[CrossRef](#)]
72. American Public Health Association (APHA); American Water Works Association; Water Environment Federation. *Standard Methods for the Examination of Water and Wastewater*, 22nd ed.; American Public Health Association: Washington, DC, USA, 2012.
73. Albano, C.; Gonzalez, J.; Ichazo, M.; Kaiser, D. Thermal stability of blends of polyolefins and sisal fiber. *Polym. Degrad. Stab.* **1999**, *66*, 179–190. [[CrossRef](#)]
74. Liu, W.; Mohanty, A.; Drzal, L.; Askel, P.; Misra, M. Effects of alkali treatment on the structure, morphology and thermal properties of native grass fibers as reinforcements for polymer matrix composites. *J. Mater. Sci.* **2004**, *39*, 1051–1054. [[CrossRef](#)]
75. Zhuo, X.; Liu, C.; Pan, R.; Dong, X.; Li, Y. Nanocellulose Mechanically Isolated from *Amorpha fruticosa* Linn. *ACS Sustain. Chem. Eng.* **2017**, *5*, 4414–4420. [[CrossRef](#)]
76. Chen, W.; Yu, H.; Liu, Y.; Hai, Y.; Zhang, M.; Chen, P. Isolation and characterization of cellulose nanofibers from four plant cellulose fibers using a chemical-ultrasonic process. *Cellulose* **2011**, *18*, 433–442. [[CrossRef](#)]
77. Corrales-Ureña, Y.R.; Villalobos-Bermúdez, C.; Pereira, R.; Camacho, M.; Estrada, E.; Argüello-Miranda, O.; Vega-Baudrit, J.R. Biogenic silica-based microparticles obtained as a sub-product of the nanocellulose extraction process from pineapple peels. *Sci. Rep.* **2018**, *8*, 10417. [[CrossRef](#)] [[PubMed](#)]
78. Sun, X.; Xu, F.; Sun, R.; Fowler, P.; Baird, M. Characteristics of degraded cellulose obtained from steam-exploded wheat straw. *Carbohydr. Res.* **2005**, *340*, 97–106. [[CrossRef](#)] [[PubMed](#)]
79. Chen, W.; Yu, H.; Liu, Y.; Chen, P.; Zhang, M.; Hai, Y. Individualization of cellulose nanofibers from wood using high-intensity ultrasonication combined with chemical pretreatments. *Carbohydr. Polym.* **2011**, *83*, 1804–1811. [[CrossRef](#)]
80. Chen, W.; Abe, K.; Uetani, K.; Yu, H.; Liu, Y.; Yano, H. Individual cotton cellulose nanofibers: Pretreatment and fibrillation technique. *Cellulose* **2014**, *21*, 1517–1528. [[CrossRef](#)]
81. Xiao, B.; Sun, X.; Sun, R. Chemical, structural, and thermal characterizations of alkali-soluble lignins and hemicelluloses, and cellulose from maize stems, rye straw, and rice straw. *Polym. Degrad. Stab.* **2001**, *74*, 307–319. [[CrossRef](#)]
82. Nishiyama, Y.; Sugiyama, J.; Chanzy, H.; Langan, P. Crystal structure and hydrogen bonding system in cellulose I α from synchrotron X-ray and neutron fiber diffraction. *J. Am. Chem. Soc.* **2003**, *125*, 14300–14306. [[CrossRef](#)]
83. Lenka, S.P.; Shaikh, W.A.; Owens, G.; Padhye, L.P.; Chakraborty, S.; Bhattacharya, T. Removal of copper from water and wastewater using dolochar. *Water Air Soil Pollut.* **2021**, *232*, 1–15. [[CrossRef](#)]
84. Ali, I.; Burakov, A.E.; Melezhhik, A.V.; Babkin, A.V.; Burakova, I.V.; Neskomornaya, M.E.A.; Galunin, E.V.; Tkachev, A.G.; Kuznetsov, D.V. Removal of copper (II) and zinc (II) ions in water on a newly synthesized polyhydroquinone/graphene nanocomposite material: Kinetics, thermodynamics and mechanism. *ChemistrySelect* **2019**, *4*, 12708–12718. [[CrossRef](#)]
85. Ghanavati, B.; Bozorgian, A.; Ghanavati, J. Removal of Copper (II) Ions from the Effluent by Carbon Nanotubes Modified with Tetrahydrofuran. *Chem. Rev. Lett.* **2022**, *5*, 68–75.
86. Bartczak, P.; Norman, M.; Klapiszewski, Ł.; Karwańska, N.; Kawalec, M.; Baczyńska, M.; Wysokowski, M.; Zdarta, J.; Ciesielczyk, F.; Jesionowski, T. Removal of nickel (II) and lead (II) ions from aqueous solution using peat as a low-cost adsorbent: A kinetic and equilibrium study. *Arab. J. Chem.* **2018**, *11*, 1209–1222. [[CrossRef](#)]
87. Al-Abbad, E.A.; Al Dwairi, R.A. Removal of nickel (II) ions from water by Jordan natural zeolite as sorbent material. *J. Saudi Chem. Soc.* **2021**, *25*, 101233. [[CrossRef](#)]
88. Zaker, Y.; Hossain, M.; Islam, T. Adsorption kinetics of methylene blue onto clay fractionated from Bijoypur soil, Bangladesh. *Res. J. Chem. Sci.* **2013**, *2231*, 606X.

Disclaimer/Publisher’s Note: The statements, opinions and data contained in all publications are solely those of the individual author(s) and contributor(s) and not of MDPI and/or the editor(s). MDPI and/or the editor(s) disclaim responsibility for any injury to people or property resulting from any ideas, methods, instructions or products referred to in the content.